Contents

List of figures II

List of tables III

1 Introduction 1
1.1 Motivation . . . 1
1.2 Troubles . . . 1
1.3 Approach . . . 2

2 Theory 3

3 Experimental 4

4 Analysis 5
4.1 Isotherm computation . . . 5
4.1.1 Volumetric isotherm . . . 5
4.1.1.1 Porosity . . . 7
4.1.1.2 Determination of the saturated vapor pressure . . . 8
4.1.1.3 Diameter error using Kelvin equation . . . 8
4.1.2 Optical measurements . . . 8
4.2 Conducted measurements . . . 9
4.3 Inhomogeneities on one wafer . . . 9
4.4 Comparison of closed and open pores . . . 13
4.4.1 Bad open pores . . . 15
4.4.2 Inverse funnelling . . . 16
4.4.2.1 Immersion experiment . . . 16
4.4.2.2 Inverse funnelling upon barrier layer dissolution . . . 16
4.4.3 Etch rate difference . . . 16
4.4.3.1 Pore opening widening pores much less than expected . . . 16
4.4.3.2 Floating experiment . . . 16
4.4.4 Do thinner membranes improve things? . . . 16
4.5 Testing theory using electron beam microscopy . . . 16
4.6 Pore size reduction using atomic layer deposition . . . 16
4.7 Isotherms proves powerful to detect and characterize defects . . . 16

Bibliography 17

List of Figures

4.1 Raw volumetric isotherm data recorded with the experimental setup as explained in **??** for one cycle without a membrane inside the cell and one with a membrane inside the cell. (a) shows the pressure values over time making the condensation and evaporation plateaus of absorption and desorption of hexane within the membrane's pores visible. (b) is the pressure loop which is relevant for the computation of the isotherms. Again, the before mentioned plateaus are visible as dips in the time derivative of the pressure. 6
4.2 (a) shows the raw data of the isotherm with membrane and interpolation of the reference isotherm without membrane. Also, the substraction of the latter (compare integrand of eq. (4.1)) is plotted where the area to be integrated for the absorption and desorption isotherm is shaded light green. The integration according to eq. (4.3) results in the isotherm displayed in (b). 7
4.3 For multiple measured membranes of the same wafer that were expected to show the same characteristics, the conducted measurements noted differences. To find possible patterns in these variations, for the newly produced wafers 295 and 296, the above shown enumeration of membranes is valid. 9
4.4 Wafer 295 and 296 processing scheme. While a signifies a recorded isotherm, the means MEB pictures have been taken. Red marks pores closed on one end, green pores open on both ends. The processed wafers are immersed in phosphoric acid for t_{immerse} or floated on for t_{float}. 10
4.5 Comparison of closed pore membranes of one wafer. (a) compares membranes of wafer 296 while fig. 4.5(b) deals with 295. 11
4.6 Comparison of open pore membranes of one wafer. (a) compares membranes of wafer 292 while fig. 4.6(b) deals with 295. 12
4.7 13
4.8 Images taken of wafer 295 during the *barrier layer* dissolution process. (a) shows milky aspects that appear after approximately twenty minutes while (b) has been taken just before removing the wafer from the acid. At this point the whole surface of the wafer is covered by phosphoric acid that passed through the pores. 15

List of Tables

4.1 Wafer specifications. The wafers thickness l_{pore}, floating time t_{float} of the *barrier layer* dissolution process and pore diameter dispersion $\Delta d_{\mathrm{pore}}^{\mathrm{MEB}}$ measured by electron beam microscopy are noted. The latter two parameters apply to the open pore membranes of the respective wafer. 9

1 Introduction

1.1 Motivation

The fundamental idea is to test models of condensation and evaporation of liquids in confinement. To this end, a well characterized confinement is neccessary. The latter shall be realized using nanoporous alumina membranes. The production of these is rather advanced as they are commonly used for the production of nanowires. Moreover, the shape of the pores is idealy cylindrical which makes for a simple geometry. A nanoporous alumina membrane includes a large number of parallel pores. Therefore, any exeriment conducted on one of these membranes yields a result that averages over all of these pores. This is why, ideally, monodisperse alumina membranes shall be produced.

As a liquid to condense inside the pores of these membranes, hexane is used. There are multiple reasons for that. First, other teams have used hexane for this type of experiments before. This means that reference isotherms exist that the results can be compared to. Moreover, hexane permits to experiment at ambient temperature which makes things much easier. The fact that this is only a preexperiment for later experiments using helium, the use of liquids like nitrogen seems to make experimenting more difficult while offering no advantages.

The models to be tested are primarily the Kelvin equation and the Saam and Cole theory. There are multiple variations though, as for example there is a modified Kelvin equation taking into account the wetting film which the basic Kelvin equation does not. In addition to that, thermal activation and the temperature relative to the critical temperature of the used fluid are relevant. The latter is one reason why finally, the experiment is planned to be conducted using helium. Finally, there are other more sphisticated models that need to be tested. Due to the small variations that are expected, again, the probing of the latter requires helium. Last but not least, in order to also study cavitation in alumina membranes, inc bottle like cavities with constricted openings must be produced. As for both, the helium experiments and for the inc bottle openings, pores of sub ten nanometer diameter must be synthesized in a controlled way, the production process needs to be improved. This becomes the main goal of the conducted experiments described in this article.

1.2 Troubles

Early on, the conducted experiments prove the membranes to be not as ideal as was hoped for. The idea of the perfect cylindrical pores of the same diameter is replaced by the conclusion that the pores' diameter is not only distributed over the membranes but also varies within a single pore. This variation manifests in the way of a funnelling aspect that makes for a conical shape, rather than a cylindrical, and also as corregations. As explained above, the confinement needs to be well characterized to be able to test the models of condensation and evaporation. In contrast to that, the geometrical shape of the pores does not allow for this kind of precise characterization. Using electron beam microscopy, the opening diameters of the pores can be checked on top and bottom side. Furthermore, a cross section view yields some information about the straightness and possible defects along the length of the pores. As the pores' length ranges in the oder of micrometers though, while the diameters' magnitude is nanometers, this still gives little information about the overall pore shape. Moreover, the microscopy images can not be precisely evaluated due to the unknown porosity of the membranes and again the lack of information on the shape. In the course of the experiments a way is developed to at least delimit a range for the porosity and so allow for a more sophisticated analysis of the electron beam microscopy images under the assumption of a certain pore geometry.

The bottom line is that neither the exact geometry and distribution of pore shapes and sizes is known, nor are the condensation and evaporation models clear. Thus, the first step must be to understand and refine the production process of the membranes and to hereby make for the best possible characterization of the confinement.

1.3 Approach

To understand the membranes' characteristics and to use this knowledge to improve the production process, rather large pore diameters of above fourty nanometer diameter, for which KELVIN equation is assumed to be sufficiently precise, are probed using multiple techniques. The core of the conducted experiments relies on thermodynamics using volumetric measurements. In addition, optical measurements and also visual documentation are used along with electron beam microscopy. All the aquired data is then interpreted and tested for coherence to finally draw conclusions on the membranes' characteristics. From the aquired results, questions rise about the effects of different production steps which are then taken a closer look at.

2 Theory

3 Experimental

4 Analysis

4.1 Isotherm computation

In the following, evaluation of the recorded raw data is presented for volumetric (section 4.1.1) and for the optical measurements (section 4.1.2).

4.1.1 Volumetric isotherm

To compute the isotherms from the recorded data the experiment needs to the conducted not only with a membrane inside of the cell, but also with an empty cell. From here on, the following indices shall be used:

$$\begin{aligned} 1 &\longrightarrow \text{no membrane} \\ 2 &\longrightarrow \text{membrane.} \end{aligned}$$

Furthermore, the variables P_i, $\dot{P}_i$, V_i, T_i, n_i and $\dot{n}_i$, $i \in \{1, 2\}$, refer to the values measured inside of the cell, in explanation the red marked part of the system in **??**. The raw isotherms of the two experiments are shown in fig. 4.1. The plateaus of the yellow curve with membrane inside the cell of the plot versus time correspond to the dips of the time derivative of the pressure of the versus pressure plot. This can be explained by the hexane condensing inside the membrane's pores at a given pressure due to which the continuing matter flow into the cell does not yield an increase of pressure.

Regarding the system with and empty cell, it is clear that the ideal gas law can be used to compute the flow rate of hexane (compare **??**). By solving for the amount of matter

$$n_1 = \frac{P_1 V_1}{R T_1},$$

taking into account that the temperature of the cell is regulated at T_1 and the volume V_1 is constant, the flow of matter becomes

$$\dot{n}_1 = \frac{V_1}{R T_1} \cdot \dot{P}_1.$$

Furthermore, the flow of matter for the system with a membrane inside the cell can be interpreted as the sum of the flow into the membrane $\dot{n}_2^{\text{mem}}$ and the flow into the system volume excluding the membrane $\dot{n}_2^{\text{cell}}$. This can be rewritten yielding

$$\dot{n}_2^{\text{mem}} = \dot{n}_2 - \dot{n}_2^{\text{cell}},$$

where $\dot{n}_2^{\text{cell}}$ obeys ideal gas law. Using the fact that the flow through the PFEIFFER valve only depends on the pressure difference $\Delta P_i = P_i^{\text{tank}} - P_i^{\text{cell}}$, assuming that $P_1^{\text{tank}} = P_2^{\text{tank}}$ leads to

$$\begin{aligned} \dot{n}_2^{\text{mem}}(P_2) &= \dot{n}_1(P_2) - \dot{n}_2^{\text{cell}}(P_2) \\ &= \frac{V_1}{R T_1} \cdot \dot{P}_1(P_2) - \frac{V_2}{R T_2} \cdot \dot{P}_2(P_2) \end{aligned} \tag{4.1}$$

Figure 4.2(a) shows the computation steps visually using the respective plots versus time.

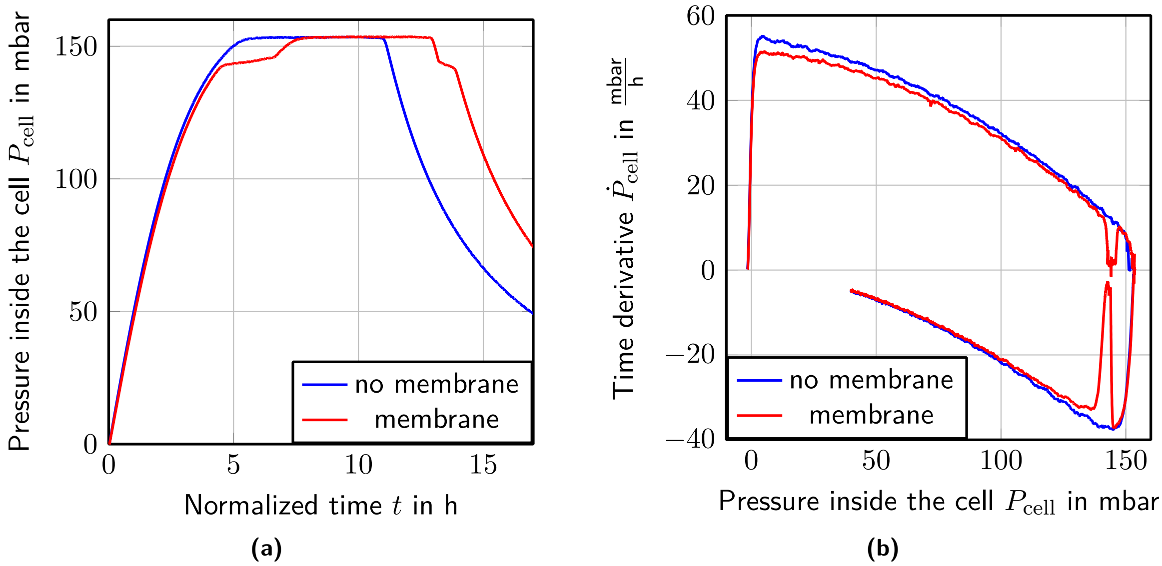

Figure 4.1 Raw volumetric isotherm data recorded with the experimental setup as explained in **??** for one cycle without a membrane inside the cell and one with a membrane inside the cell. (a) shows the pressure values over time making the condensation and evaporation plateaus of absorption and desorption of hexane within the membrane's pores visible. (b) is the pressure loop which is relevant for the computation of the isotherms. Again, the before mentioned plateaus are visible as dips in the time derivative of the pressure.

As the temperature of the system is regulated ($T = T_1 = T_2 = \mathrm{const.}$) and because $V = V_1 \approx V_2$ since $V_{\mathrm{mem}} \ll V_1$, equation eq. (4.1) yields

$$n_2^{\mathrm{membrane}} = \frac{V}{RT} \int_0^{t_2} \left(\dot{P}_1(t_1') - \dot{P}_2(t_2') \right) \mathrm{d}t_2'. \tag{4.2}$$

Important at this point is the dependency of $\dot{P}_1(t_1)$ on t_1) while the integration is over t_2.

As the experimental setup yields discreet values at given time intervals Δt, the data evaluation makes use of a sum rather than an integration.

$$n = \frac{V}{RT} \sum \left(\dot{P}_1(P_1 = P_2) - \dot{P}_2(P_2) \right) \cdot \Delta t \tag{4.3}$$

yields the molar amount of hexane condensed inside the membrane. Figure fig. 4.2(b) shows the result of the integration eq. (4.3) for membrane 296d. It is a absorption and desorption isotherm for hexane inside the porous alumina membrane. The bulk condensation and evaporation is not visible, as it is also recorded with the reference isotherm without membrane inside the cell.

What stings the eye is that the sharp rise of the condensation branch does not start at the liquid fraction $LF = 0$. The same goes for the evaporation branch. It only drops to a liquid fraction value $LF > 0$ and then decreases superimposed with the condensation branch. While is would be reasonable to renormalize the graph so only the mentioned sharp rise and drop are relevant for the isotherm as this part is where the pores fill or empty at spinodal or equilibrium pressure (**??**), it is not done here. The reason for this is that the initial rise of the isotherms is assumed to be due to the build up of a film on the membranes surfaces. This is part of the theory of condensation and evaporation in confinement even though the film is ignored in the basic KELVIN equation (**??**). ???MAKE A COMPUTATION AS TO HOW MANY MOLES OF LIQUID ARE EXPECTED FOR THE FILMS ON ONE SINGLE MEMBRANE???

Moreover, the plots

$$i \quad \text{over} \quad j, \quad i \in \{n, LF, FF\}, \quad j \in \{P_{\mathrm{cell}}, P_{\mathrm{rel}}, D_{\mathrm{kelvin}}\} \tag{4.4}$$

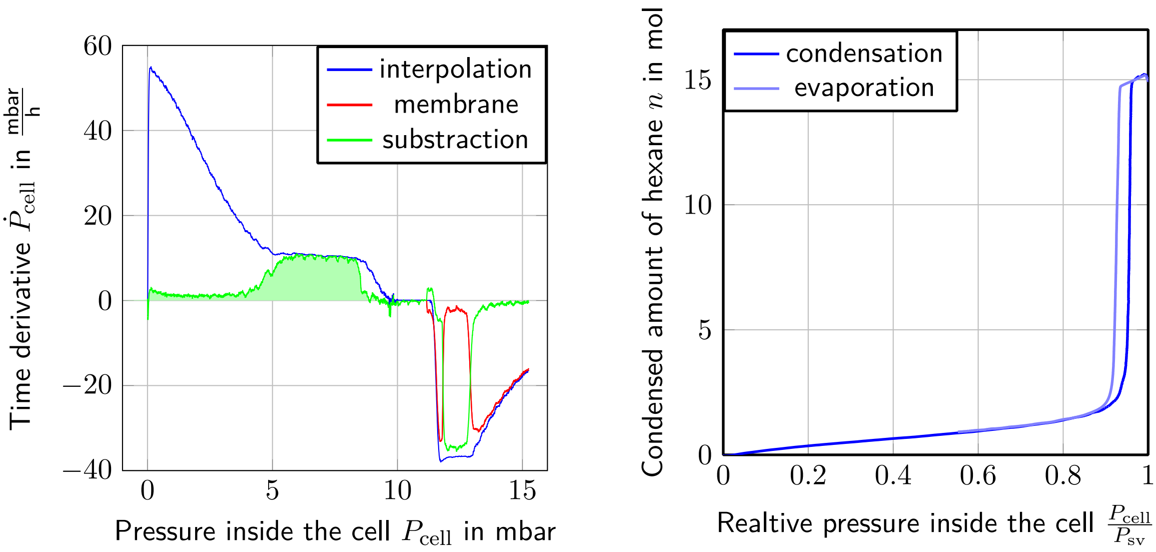

(a) **(b)**

Figure 4.2 (a) shows the raw data of the isotherm with membrane and interpolation of the reference isotherm without membrane. Also, the substraction of the latter (compare integrand of eq. (4.1)) is plotted where the area to be integrated for the absorption and desorption isotherm is shaded light green. The integration according to eq. (4.3) results in the isotherm displayed in (b).

are of interest, where

$$P_{\text{rel}} = \frac{P_{\text{cell}}}{P_{\text{sv}}^{\text{exp}}}, \tag{4.5}$$

with the saturated vapor pressure P_{sv}.

$$LF = \frac{n}{n_{\text{max}}} \tag{4.6}$$

is the liquid fraction of hexane condensed inside the pores of the membrane using the total maximum amount of condensed hexane n_{max} and last,

$$FF = \frac{V_{\text{hex}}^{\text{cond}}}{V_{\text{mem}}} \tag{4.7}$$

with the volume of condensed hexane $V_{\text{hex}}^{\text{cond}}$ and the membrane's volume V_{mem}, is the filled fraction of the membrane. Its maximum corresponds to the porosity of the membrane. For the computation please refer to **??**.

For the computation of the introduced physical sizes, the saturated vapor pressure P_{sv} must be determined.

4.1.1.1 Porosity

Equation eq. (4.3) gives the molar amount of hexane n_{hex} condensed inside the membrane's pores. Furthermore, for the given pressures 0 mbarto160 mbar hexane in its liquid form can be regarded as incompressible and therefore the hexane's volume be computed via

$$V_{\text{hex}} = n_{\text{hex}} \cdot V_{\text{mol,hex}}.$$

. The thickness l_{pore} of the membrane is easily determinable via MEB views since its magnitude is micrometers. Finally, the area A_{mem} of the measured samples is derived from a photo taken using binoculars.

Using these information the porosity ϕ of a given membrane is given by

$$\phi = 1 - \frac{V_{\text{hex}}}{V_{\text{mem}}}, \tag{4.8}$$

with the membrane's volume

$$V_{\text{mem}} = A_{\text{mem}} \cdot l_{\text{pore}}.$$

4.1.1.2 Determination of the saturated vapor pressure

As the bulk condensation plateau shows a slight drift (compare figure fig. 4.1), using the maximum measured pressure P_{cell} does not yield the saturated vapor pressure P_{sv} but a higher value. In addition, depending on the contamination of the system by air or degassing grease, the measured value for P_{sv} shifts due to the partial pressures. To probe the reproducibility of an isotherm loop including the grade of contamination, the node[anchor=south]maximum measured pressure for different membranes is compared. As the system is opened to replace the membrane in between the isotherms, each cycle is independent. For the change of membrane process please read **??**. The result of the experiment is that $P_{\text{sv}}^{\text{exp}}$ fluctuates by

$$\delta P_{\text{sv}}^{\text{exp}} = \pm 0{,}5\,\text{mbar}. \tag{4.9}$$

As the relevant plateau of condensation and evaporation inside the pores of the membrane occur at about

$$P_{\text{plateaus}} = 140\,\text{mbar}, \tag{4.10}$$

$\delta P_{\text{sv}}^{\text{exp}}$ translates to an error of about

$$\delta P_{\text{rel}} \leq \pm 0,005. \tag{4.11}$$

4.1.1.3 Diameter error using Kelvin equation

Gaussian error propagation to check the precision of the experiment.

4.1.2 Optical measurements

As mentioned in **??**, the light transmission setup is independent from the volumetric measurements and also the evaluations do not depend on each other. The light transmission is rather a tool to check on the theory of evaporation and condensation within the membrane using a different approach.

To compute the transmission coefficient of a membrane, it is measured in dry state using the same transmission setup as during the volumetric experiment yielding $T_{\text{mem}}^{\text{dry}}$. Then, the first measured intensity value I_0 of a given isotherm is assigned to the dry coefficient as at this point no hexane is condensed inside of the membranes pores yet. From there on, each intensity measurement is translated to a transmission coefficient according to

$$T(t) = T_{\text{mem}}^{\text{dry}} \cdot \frac{I_0}{I(t)}. \tag{4.12}$$

The aquired physical size can be interpreted as explained in the following **??**.

As a forword shall be mentioned that the observed transmission drops' magnitude cannot be explained by simple media transmissions as explained in **??**. Even counting multiple transitions for a diagonal transmission of a membrane, the regular transmission is not a sufficient explanation as the filled state of a membrane should by that theory be less transmitting than the empty state whereas the opposite is observed. To explain the phenomena, Rayleigh scattering and index matching, which are explained in **??** and **??** respectively, must be taken into account.

4.2 Conducted measurements

Genereal: From one wafer we can test different things as we have 12 membranes. Wafer produced as a whole so membranes should be equivalent. ADD THE CIRCLE HERE!!!

Membranes of four different wafers produced according to **??** have been measured. The wafers specifications are noted in table 4.1. As multiple membranes in the same state of the same wafer yielded different results, the position of the single membranes on the wafer were are taken note for newly produced wafers. Therefore, for the wafers 295 and 296, the membranes' names correspond to the positions shown in fig. 4.3. Furthermore, all conducted measurements on the membranes in different states are noted on fig. 4.4.

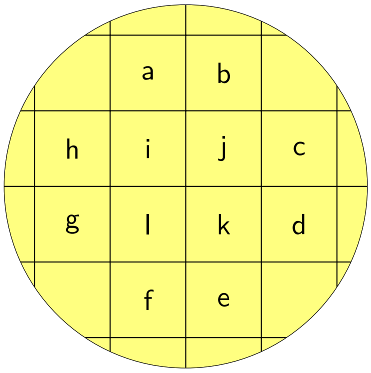

Figure 4.3 For multiple measured membranes of the same wafer that were expected to show the same characteristics, the conducted measurements noted differences. To find possible patterns in these variations, for the newly produced wafers 295 and 296, the above shown enumeration of membranes is valid.

Table 4.1 Wafer specifications. The wafers thickness l_{pore}, floating time t_{float} of the *barrier layer* dissolution process and pore diameter dispersion $\Delta d_{\mathrm{pore}}^{\mathrm{MEB}}$ measured by electron beam microscopy are noted. The latter two parameters apply to the open pore membranes of the respective wafer.

Wafer	l_{pore} [µm]	t_{float} [min]	$\Delta d_{\mathrm{pore}}^{\mathrm{MEB}}$ [nm]
292	60	0	
294	60	0	
295	60	35	
296	30	40	7

4.3 Inhomogeneities on one wafer

To start with, the wafers shall be tested for inhomogeneities. Therefore, isotherms of one wafer's membranes which are in the same technical state, meaning they have undergone exactly the same treatments, asrae compared. This is done for both, closed pore membranes and open pore membranes. Because opening the membranes' pores involves one more production step, here, closed pore membranes are regarded first.

Figure 4.5 shows a comparison of closed pore membranes for wafer 295 and 296. Even though the membranes 296e' and 296f' had already been treated using phosphoric acid at the time of the measurements, the pores are still assumed to be closed as will be explained in section 4.4.

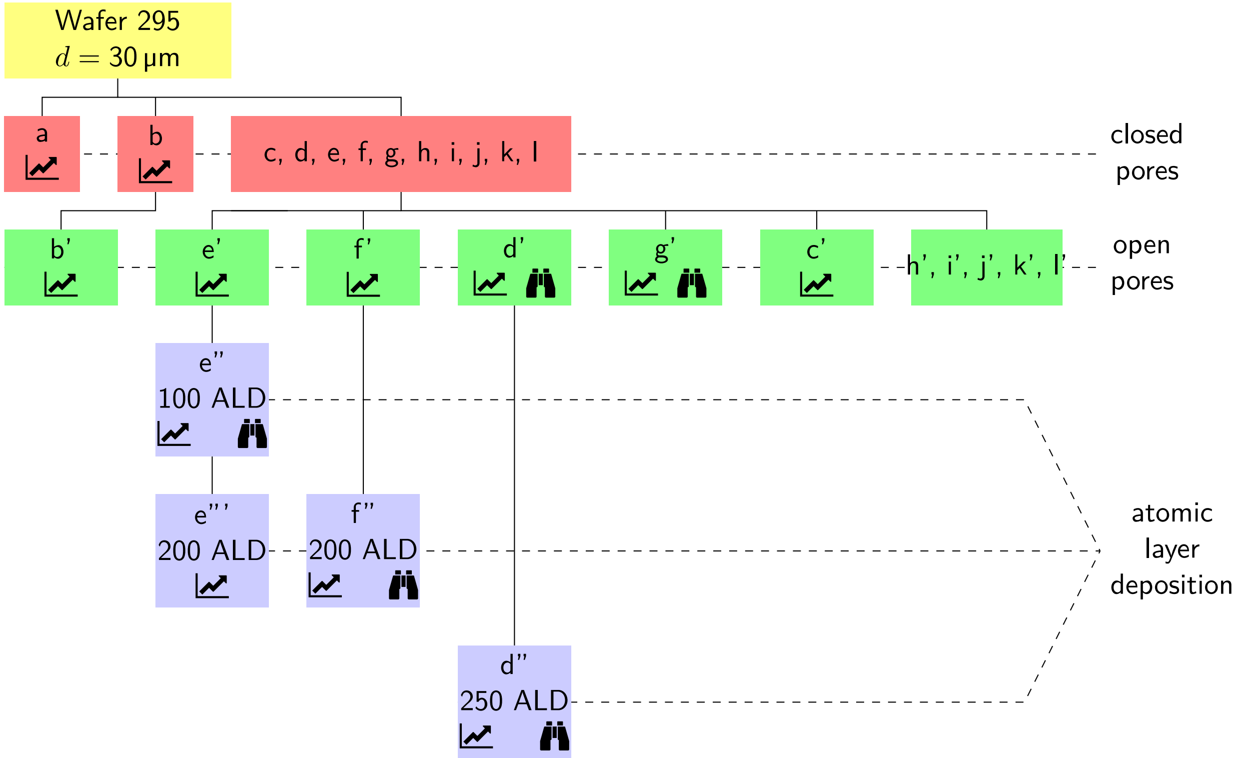

(a)

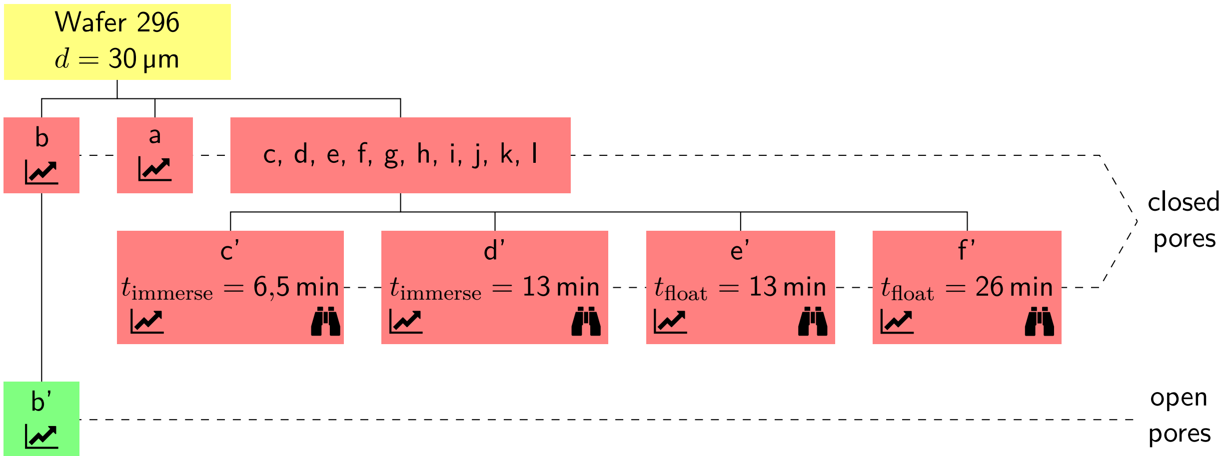

(b)

Figure 4.4 Wafer 295 and 296 processing scheme. While a signifies a recorded isotherm, the means MEB pictures have been taken. Red marks pores closed on one end, green pores open on both ends. The processed wafers are immersed in phosphoric acid for t_{immerse} or floated on for t_{float}.

While for both wafers, with one exception being membrane 295c, the overall shape of the different membranes' volumetric isotherms matches, they are distributed along a short distance of the P_{rel}-axis. As long as the shapes and also the size of the hysteresis match, this can be explained by a differing pore size distribution for the different membranes. NEED DIAMETER CONVERSION FOR THIS??? Membrane 295c shall not be analysed at this point as it will be dealt with in detail in section 4.7. Moreover, also the transmission measuremens yield optical signals of similar shapes. Unclear at this point is the variation in magnitude that can be extreme for some membranes as the example of 296f' compared to 296b shows.

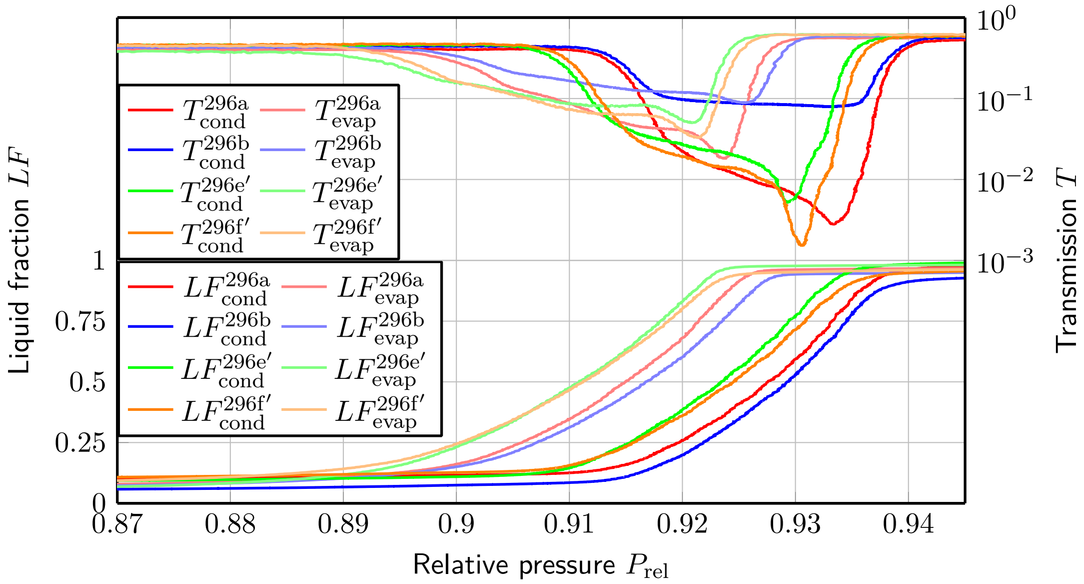

(a)

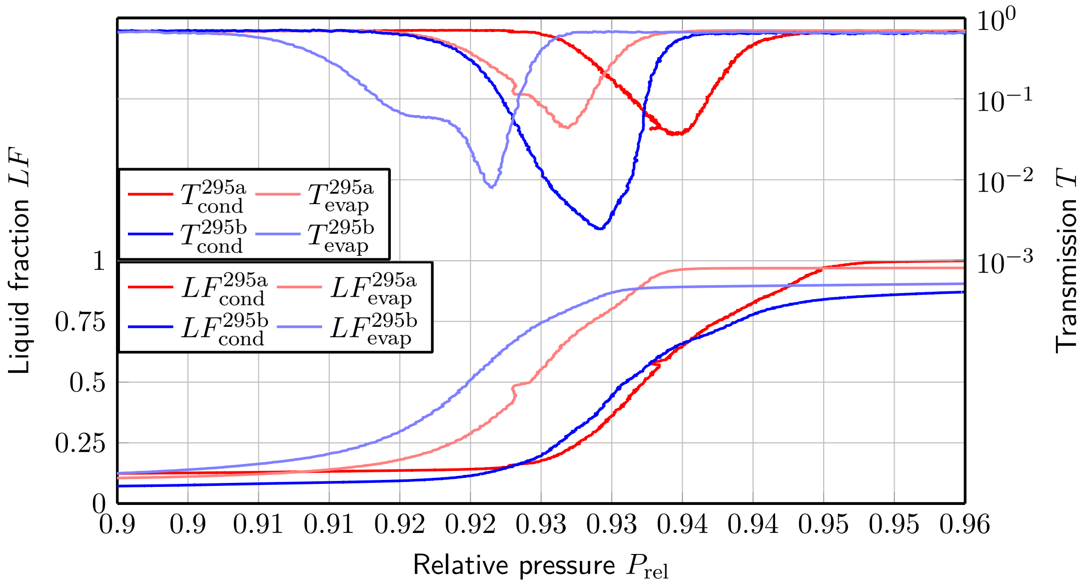

(b)

Figure 4.5 Comparison of closed pore membranes of one wafer. (a) compares membranes of wafer 296 while fig. 4.5(b) deals with 295.

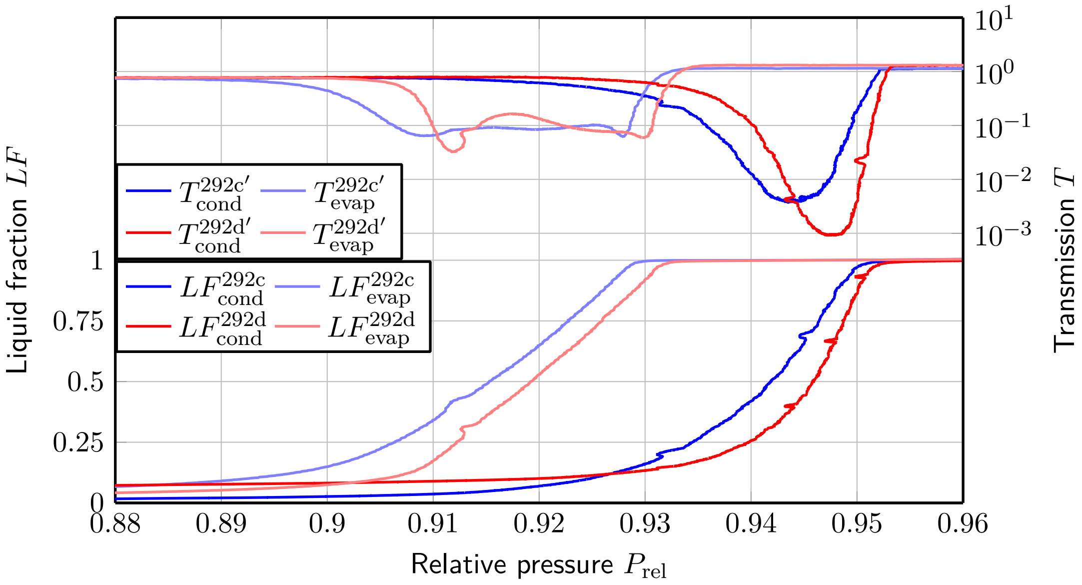

(a)

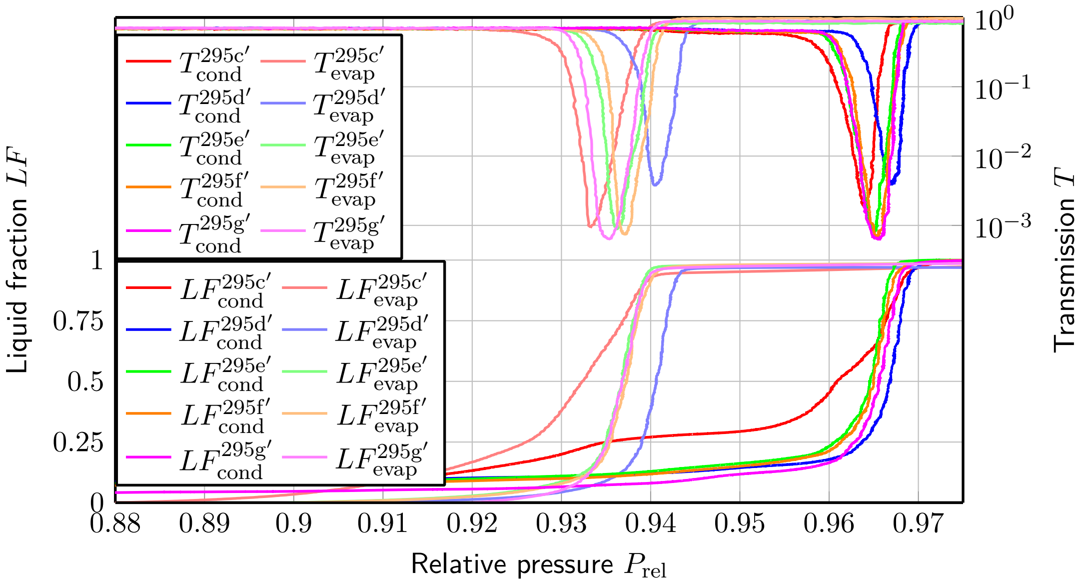

(b)

Figure 4.6 Comparison of open pore membranes of one wafer. (a) compares membranes of wafer 292 while fig. 4.6(b) deals with 295.

4.4 Comparison of closed and open pores

Show comparison of 294, 295 and 296. Speak about the context to theory. Testing the efficiency of opening procedure. Theory test relies on the fact that pores are well open. ADD ONE THAT DID NOT WORK

Hysteresis for closed: corrugations

Hysteresis difference: Coherent with theory

This section shall serve to determine a systematic change of the isotherm by the *barrier layer* dissolution process which opens the pores on the bottom side. Moreover, the coherence with theory shall be regarded. Figure 4.7 shows the comparisons of closed pore and open pore membranes of the wafers 295 and 296. For both, closed and open pore measurements, the same membranes are used before and after the *barrier layer* dissolution to leave no doubt as to the inhomogeneities of the wafers.

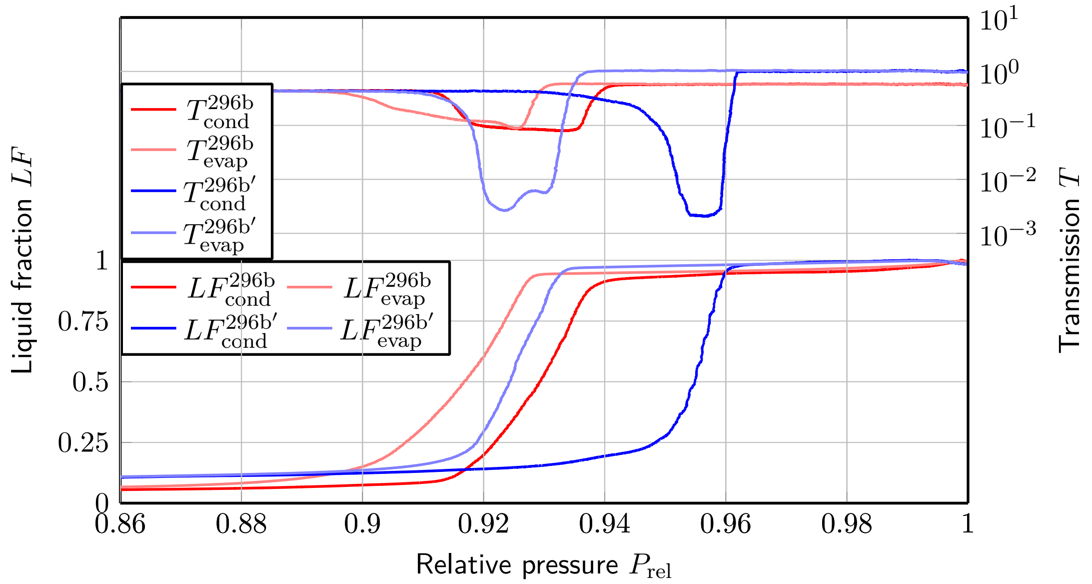

(a)

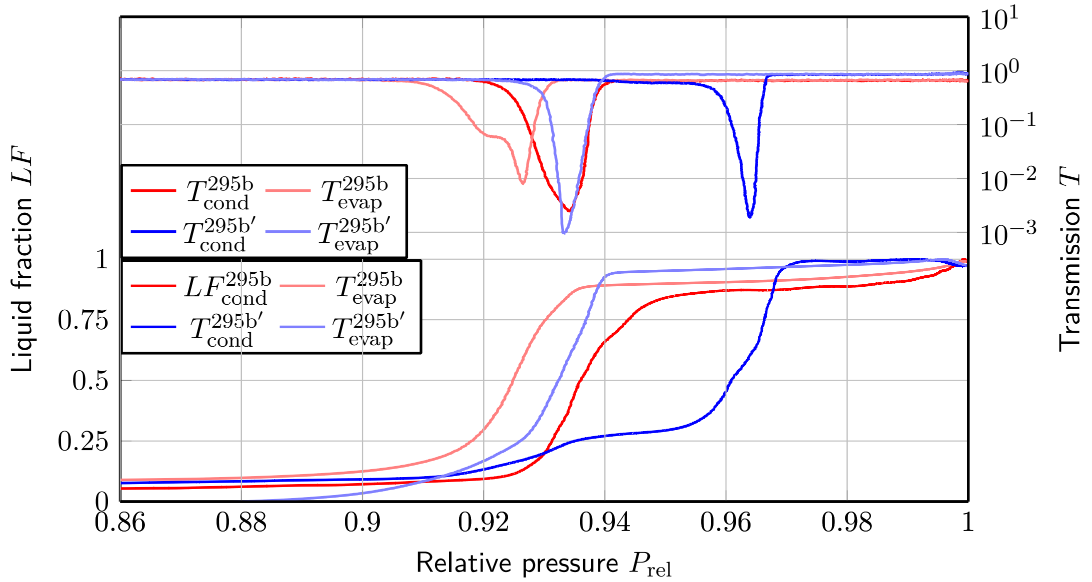

(b)

Figure 4.7

Firstly, in reference to the model explained in **??**, the occurence of a hysteresis for the volumetric isotherm of a closed pore membrane must be explained. The answer to that question has already been given by (???cite bruschi???): It occurs due to intra pore corrugations. The modulation of the diameter along the pore's length corresponds to a varying equilibrium pressure. This makes for a non vertical isotherm.

Next,the difference between the isotherms for closed and open pores is regarded. Clearly, the size of the hysteresis increases. This tendency is coherent with theory as the latter predicts a hysteresis for open pores but as mentioned above, none for closed pores. Moreover, the evaporation branch of the open pore isotherm is shifted towards higher pressures as compared to the closed pore isotherm. That implies an increase of the pore diameter upon dissolving the *barrier layer*. What stings the eye of the attentive reader is that the evaporation branch also becomes more sharp for the open pores.

An explanation of the latter two phenomena can be taken from the production step of the *barrier layer* dissolution. As displayed in fig. 4.8(a), the wafer at some point becomes milky. Comparing these milky aspects to images taken during the condensation process of an isotherm as displayed in ??? leads to the conclusion, that at this point some of the pores start filling or are already filled with phosphoric acid. This phenomena lasting for a couple of minutes is followed by fifteen more minutes of floating until the wafer is completely covered by acid that flowed through the now open pores (compare fig. 4.8(b)). That means during at least

$$t_{\mathrm{filled}} = 15\,\mathrm{min} \tag{4.13}$$

the pores are filled by phosphoric acid. That at the end of the process, the wafer is covered by a clearly visible layer of acid, means that there must be some flux of acid through the pores. On the other hand, taking into account the sharpening evaporation branch of the volumetric isotherms implies either a sharpening pore size distribution or a decrease of the funnellization or corrugation aspect of the pores.

By linking the occuring milky aspects to the filling of only some of the pores, meaning not all pores fill at the same time but over a span of

$$t_{\mathrm{milky}} = 3\,\mathrm{min}, \tag{4.14}$$

implies that the pore size distribution should rather be increased than decreased. Excluding this point only leaves corrugations and funnellization as explanations for the sharpening isotherms. As there is no reason to believe that an etching process could flatten a corrugated surface though, the straightening of the pores is more likely. Moreover, this inverse funnelling could be explained by the acid saturating along the axis of the pores. The theory of inverse funnelling is probed by experiments that will be analysed in section 4.4.2.

As the thickness of the *barrier layer* of wafer 292 has been determined to be

$$d_{\mathrm{barrier-layer}} = 30\,\mathrm{nm} \tag{4.15}$$

though, the theory introduced above raises questions regarding the etch rate of phosphoric acid on alumina. That the milky aspects appeared after

$$t^{292}_{\mathrm{float}} = 20\,\mathrm{min} \tag{4.16}$$

,which is the time after which the *barrier layer* is assumed to be etched off the wafer, makes for an etch rate of

$$e = 1{,}5\,\frac{\mathrm{nm}}{\mathrm{min}}. \tag{4.17}$$

During the fifteen minutes etching of filled pores, this would make an increase of pore diameters of

$$\Delta d_{\mathrm{pore}} = 22{,}5\,\mathrm{nm} \tag{4.18}$$

disregarding the acid saturation within the pores. Nevertheless, even regarding the saturation, the bottom end of the pores that is exposed to the bulk acid reservoir should be widened dramatically.

Calibrating the etch rates parallel to the pore axis $e_{\|}$ and perpendicular to the axis e_{perp} is another goal of the experiments.

As a way to not increase the distribution of pore diameters on a given wafer, the idea of floating the wafer on acid for a time just short enough to not open any pores, followed by its full immersion in acid has been developed. As to not increase the pores diameter by too much regardless of the acids saturation, the immediate immersion of the whole wafer wihtout prefloating discarded. Again, the acid's etch rate on the *barrier layer* is a prerequisite and shall be deduced in section 4.4.3.

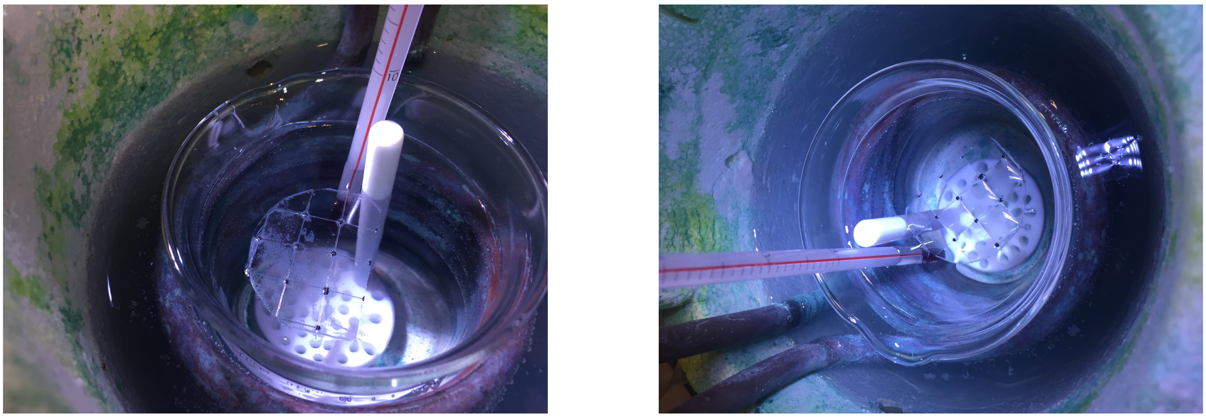

(a) **(b)**

Figure 4.8 Images taken of wafer 295 during the *barrier layer* dissolution process. (a) shows milky aspects that appear after approximately twenty minutes while (b) has been taken just before removing the wafer from the acid. At this point the whole surface of the wafer is covered by phosphoric acid that passed through the pores.

Firstly, . As expected from **??**, the hysteresis is much larger for open pores than it is for closed pores.

?? shows a full comparison of the volumetric measurements of the membranes mentioned above. Additionally, membrane 296a (closed pores) and 296b before and after the barrier layer dissolution are presented on the graph. So the membranes 296a and 296b cp serve as reference for closed pore membranes, while 296b op serves for open pore membranes. The comparison of the different membranes yields a significant difference of the hysteresis' size of 296b op and all other membranes, which show a much smaller hysteresis. As the size of the hysteresis for the rest of the membranes is approcimately uniform and the variation of the condensation and evaporation pressures are only slighty shifted, this implies that indeed, all membranes except 296b op contain pores open only on one end. Which cannot be observed though, that is weather the pores already have microscopic openings on the barrier layer side. If that were the case, hexane would condense there at spinodal pressures lower than the equilibrium pressure of the small ends. Hereby, the pores would be left in a closed shape. This case would not be visible on the volumetric measurements as the condensed amount of hexane necessary to close the pores were so small. If the openings were so large already as for the spinodal pressure to be larger than the equilibrium pressure of the small end, that case would be visible on the isotherm because whole pores would fill at higher pressures. Therefore, the latter case can be excluded.

4.4.1 Bad open pores

Talks about 294 and leads to

4.4.2 Inverse funnelling

4.4.2.1 Immersion experiment

Derive and explain etch rate gradient and influence on the pores' shape.

4.4.2.2 Inverse funnelling upon barrier layer dissolution

Explain that the pores appear to be straightened bc of floating. Refer to the theory, that there are two sorts of alumina (pure and acid polluted).

4.4.3 Etch rate difference

Introduce the conducted experiments shortly.

4.4.3.1 Pore opening widening pores much less than expected

Use the example of 292d to explain that the etch rate along the pore axis must be different from the radial one. Conclusion: etch rate offset!S

4.4.3.2 Floating experiment

Explan that the shapes of the isotherms are correct, but that no real conlusion could be made due to the bad MEB views.

4.4.4 Do thinner membranes improve things?

Compare 295 and 296. Talk about the sharpness of both, the volumetric and the optical isotherm. Also speak about the rather broad isotherm for closed pores of 295 which is not understood. Use diameter translation by Kelvin law!!

4.5 Testing theory using electron beam microscopy

4.6 Pore size reduction using atomic layer deposition

4.7 Isotherms proves powerful to detect and characterize defects

Bring up membrane 293 (constricted pore ends) and membrane 295c (closed pores).

Bibliography

[Cd15] Universität Konstanz: Corporate Design Manual. Universtät Konstanz, (2015)